Microplasma Trapping of Particles

J. Xue and J. Hopwood
Electrical and Computer Engineering, Tufts University
161 College Avenue, Medford, Massachusetts 02155 USA
Email: hopwood@ece.tufts.edu

***Abstract*—The localized potential gradients created by a microplasma are capable of trapping and concentrating micro- and nanoparticles. In this work, argon microplasma is generated within a 350 μm discharge gap formed within a microstrip transmission line. Melamine formaldehyde particles (1 μm) are released approximately 2 cm away from the microplasma. The microparticles are then negatively charged by stray electrons, electrostatically drawn toward the potential well of the microplasma, and trapped within the microplasma. The particles are observed to form Coulomb crystals. Time-of-flight experiments show that the particles are trapped in the microplasma by balancing the electrostatic force of the potential well against the molecular drag force. Pulsed plasma data show that the particles retain a net negative charge after the plasma has been extinguished, allowing detection and sorting by electrostatic methods**

***Index Terms*—Microplasma, Microparticle, dusty plasma.**

I. Introduction

THERE is a basic need for accurate detection of nanoparticles in the environment, and in particular, for detection of airborne particles that may affect human health. In this application, a portable detection system is preferred over laboratory instrumentation. Detection of nanoparticles and the determination of their size distribution is also a critical diagnostic tool for nanomanufacturing processes that are expected to produce close-tolerance nanoparticles. Manufacturing processes that require the use of nanoparticles as a raw material may also benefit from the development of sensors capable of monitoring the size distribution of the source materials in real time. Finally, the downward scaling of critical dimensions in integrated microelectronics requires the detection of nanometer-size particles that cause killer defects in deep submicron chip structures.

Particle classification is commonly performed using a differential mobility analyzer (DMA) in which particles are charged and then segregated based on particle electrical mobility [1]. The ionization of the particles is typically performed by bipolar diffusion charging using a Kr-85 [1] or Po-210 source [2]. The use of radioisotopes produces a well characterized bipolar charge distribution, but strictly limits the portability of the particle analyzer due to rules governing the tracking of these hazardous materials.

The physics of particles in plasmas has been extensively studied [3], and the recent strong interest in plasma-particle interactions is motivated by the unwanted production of particles in plasma systems used for the fabrication of microelectronics [4]. Isolated bodies in electropositive plasma are well-known to accumulate a net negative charge. This is because free electrons in the plasma have much higher mobility and temperature than positive ions. The collection of electrons on the surface of a particle proceeds until the surface potential is sufficiently negative that additional electrons are electrostatically repelled. In the steady-state, the fluxes of electrons and positive ions to a particle must balance. This observation leads to the commonly used although somewhat oversimplified [5], [6], [7], [8] expression for the charge on a particle immersed in a plasma with density n_e and electron temperature T_e,

$$\sqrt{\frac{T_e m_i}{T_i m_e}} exp(\frac{-e^2 Z_d}{4\pi\varepsilon_0 a K_B T_e}) = (1 + \frac{Z_d n_d}{n_e})(1 + \frac{e^2 Z_d}{4\pi\varepsilon_0 a K_B T_i}) \quad (1)$$

where Z_d is the charge on a particle in units of electron charges and a is the radius of the particle [9]. From this implicit equation it is possible to observe that the charge on a particle is proportional to the particle radius ($Z_d/a \cong const$) and is independent of the plasma density if the nanoparticle charge density is much less than the electron density ($Z_d n_d << n_e$). This condition is easily satisfied by limiting the number of particles within the plasma. As a concrete example, a 10 nm particle will accumulate ~35 excess electrons in a plasma with $T_e = 2eV$, and a 1 μm particle used in this paper will accumulate 3500 excess electrons. Electronegative plasmas containing significant densities of negative ions will modify the charging of particles, as will photoemission of electrons from the particle surface. Nonetheless, plasma charging of particles presents a reasonable alternative to the use of radioisotopes, albeit with a substantially higher, unipolar charge distribution.

Most plasma generators are too large and expensive for portable sensor applications. In this work, we investigate an alternate method of particle charging by using microplasma. The advent of plasma displays has resulted in the widespread use of microplasmas since each display pixel consists of a microscopic gas discharge. In parallel with display research, however, a growing number of labs are investigating microplasma generation as an excitation source for portable sensors and chemical analysis. This body of work has been summarized by Karanassios [10] and includes examples of atomic emission spectrometry and mass spectrometry using microplasma excitation sources. Giapis' group [11] has also reported using a microplasma to create silicon nanoparticles through short residence-time growth. These particles were 1-3 nm in size and also exhibited charging from the microplasma. Here, we report on the particle behavior in a so-called plasma-

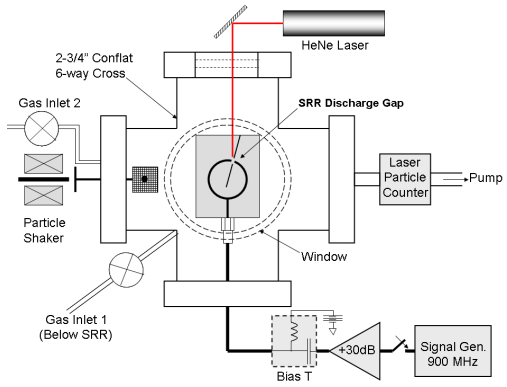

Fig. 1. Experiment set up

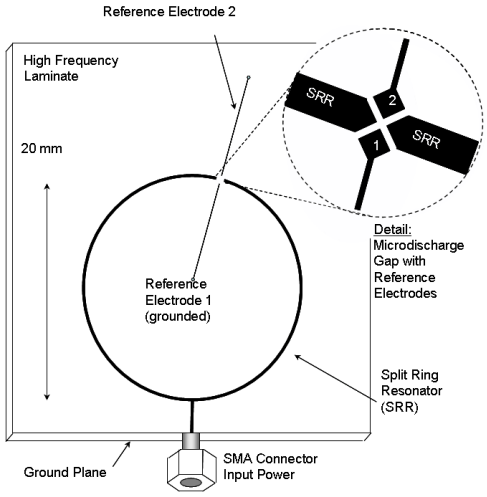

Fig. 2. Split Ring Resonator(SRR) and Reference Electrodes

on-a-chip.

II. EXPERIMENT

The experimental microplasma apparatus resides in a 2-3/4" conflat 6-way cross (see Fig. 1). The microplasma is generated by a microstrip transmission line formed into a split ring resonator (SRR) as shown in Fig. 2 [12]. Microwave power applied to the SRR at its resonant frequency of 900 MHz causes a large voltage to form across the 350 μm discharge gap in the split ring, and a stable microplasma is formed. Due to the symmetric excitation of the SRR, the copper electrode surfaces that form the gap are at the same DC potential. The absence of high DC voltages reduces or eliminates electrode erosion by energetic ions. The SRR is micromachined in copper-clad laminate (R/T Duroid 6010.2) using an $LPKF$ $Protomat$® circuit prototyping tool. In this experiment, there are two argon flow inlets. The first inlet is located behind the microplasma generator. The second inlet is mounted adjacent to the particle source (see Fig. 1). The ambient pressure is measured using a capacitance manometer.

If needed, a bias voltage can be applied to the entire SRR structure through a Bias T as shown in Fig. 1. Two grounded reference electrodes are micromachined on the surface of the SRR and each electrode contacts the microplasma in the region of the discharge gap (see Fig. 2). The gap between the reference electrode and the split ring tip is 150 μm. The opposite end of each electrode is grounded to the underlying ground plane by a conducting via through the laminate. The length of these two electrodes is designed such that their input impedance at 900 MHz is large ($\sim \lambda/4$), and therefore the electrodes do not interfere with the operation of the resonator. These two electrode surfaces provide a ground reference against which the DC potential of the SRR can be modified using the Bias T.

Melamine formaldehyde spheres (Corpuscular Inc., ♯$360211-10$, dry, 1 μm diam. mass density $1.51 g.cm^{-3}$) are introduced into the experiment through a 'shaker'. The shaker consists of an aluminum vessel that has been drilled with a single outlet hole (0.050") in one side. To reduce agglomeration of particles, the outlet hole is covered by a nickel mesh with 6 μm openings. The shaker is mounted on a linear feedthrough, and particles are released by striking the external side of the shaker using a solenoid.

The particles are observed and photographed through an observation window above the microplasma. A HeNe laser beam enters the test chamber at 90° to the observation window such that light scattered from the particles can be photographed using a digital camera mounted on a microscope with a long working distance. A 632 nm bandpass filter is used to block light emission from the microplasma during photography. In addition to simply observing particles trapped by the plasma, particles can also be counted using a laser particle counter located at the pumping port of the test chamber (Fig. 1). A data acquisition board controlled by a Labview program is used to control the plasma, release particles, and read the particle counter signal.

III. RESULTS AND DISCUSSION

A. Basic plasma data

The plasma properties presented in this section were obtained with a coaxial Langmuir probe in which the inner conductor (silver-coated 0.008" in diameter) acts as one of the probes and the outer conductor (copper 0.034" in diameter) as the other probe. A voltage-current curve was obtained by sweeping the voltage across the probe and recording the current flowing through the probes at each voltage. Electron temperature and plasma density were calculated by an iterative process [19] using collisional probe theory. The results are posted in Table 1.

TABLE I
BASIC PLASMA DATA

Pressure (Torr)	Power (W)	T_e (eV)	$n_i(\mathrm{cm}^{-3})$
4	0.45	1.6	1.4×10^{11}
4	0.25	1.6	1.2×10^{11}
2	0.25	1.7	1.3×10^{11}

The electron temperature (T_e) decreases with increasing pressure, because the electron diffusion decreases as the number of collisions increases, so T_e at 2 Torr is higher than at 4 Torr. Electron temperature is independent of plasma density, in other words it is independent of input power. At same

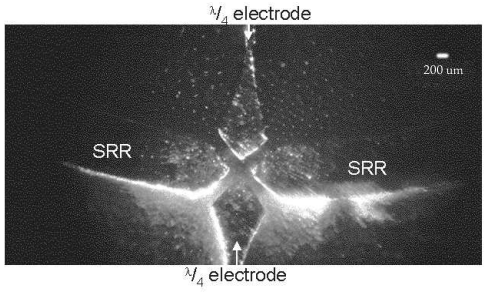

Fig. 3. Photograph of particles suspending in a 2 Torr argon microplasma

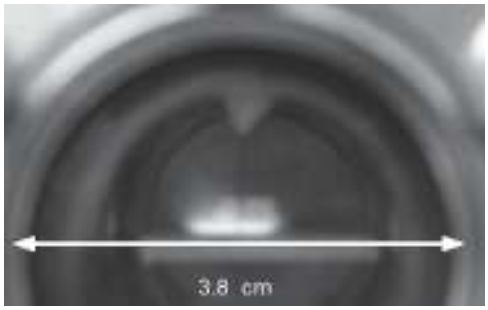

Fig. 4. Photograph of a 2 Torr argon microplasma viewed through the 3.8 cm side window

pressure, as input power is increased from 0.25 w to 0.45 w, the electron density increases but the electron temperature remains constant.

B. Particle Behavior

Particles suspended in a 2 Torr argon microplasma can be observed in Fig. 3. Because the lower quadrants of the substrate are illuminated by the laser light, only the particles in the upper quadrants are visible. Here we used inlet 1 to introduce argon gas to ensure that particles were trapped in microplasma and not swept away by gas flow. These particles and the microplasma electrodes are illuminated by the HeNe laser light source that enters from the lower edge of the photograph. The two electrodes of the split ring resonator are labeled 'SRR' in the photograph and the reference electrodes ($\lambda/4$) extend vertically from the 350 μm discharge gap. The microplasma glow is not visible due to a 632 nm filter used during the experiment, but the size of the discharge, as viewed from the side window, can be seen in Fig. 4.

The particles were introduced into the microplasma by tapping the shaker that was located 2 cm to side of the microplasma. It is believed that stray electrons from the microplasma rapidly charge the particles [13] and the charged particles are accelerated toward the microplasma by the electrostatic potential well formed in the discharge. The potential well exists because highly mobile electrons diffuse from the microplasma more rapidly than the positive ions. This leaves the central volume of the microplasma with a higher potential than the surrounding region [14]. Particles are observed to arrive and become trapped in the microplasma on the order of 1 second after their release from the shaker.

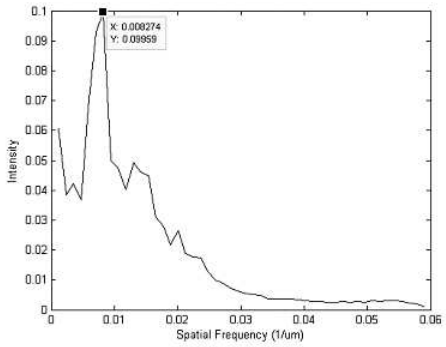

Fig. 5. Spacial frequency determined by two-dimensional fast Fourier transform of the image(Fig. 3) and integrating the FFT in the K_ϕ direction.

In this plasma, the dominant forces acting on the microparticles are molecule drag force due to the argon gas flow, electrostatic forces due to the electric fields in the sheath and the electrostatic potential well, ion drag force due to the flux of ions flowing toward the substrate and gravitational force. The gravitational force is about $7.7 \times 10^{-15} N$, the molecule drag force is on the order of $10^{-14} N$, and both the ion drag force and electrostatic force in the sheath are on the order of $10^{-12} N$. Due to the small particle size and the high ion density of the microplasma, the gravitational force is negligible. In fact, the microplasma can be rotated a full 360° and functions independently of spatial orientation. This is distinct from many other dusty laboratory plasmas where the gravitational force is important due to larger particles and lower ion drag force due to minimal ion density ($\sim 10^8 cm^{-3}$). In the horizontal direction, the molecule drag force is balanced by the electric field force in the electrostatic potential well. In the vertical direction, the electrostatic force in the sheath is balanced by the ion drag force. So all of the trapped particles are suspended in the discharge above the dielectric substrate, which consists of TiO_2-polymer composite.

Particles in the upper left quadrant of Fig. 3 are in motion and appear as short streaks in this 0.1 s exposure. The particles in the right upper quadrant, however, have reached equilibrium positions and formed a Coulomb crystal. Fig. 5 shows the periodicity of the Coulomb crystal is 120 microns. The spatial frequency was determined by taking the two-dimensional fast Fourier transform of the image and integrating the FFT in the k_ϕ direction. It is interesting to note that these two populations of particles are isolated by the linear potential barrier of the grounded reference electrode. Similar plasma crystals have been created using large scale capacitively coupled plasma (CCP) generators. In the CCP, particles are typically suspended above an rf powered electrode by the steep potential gradient of the plasma sheath. The particles are held in a position near the sheath where the ion drag force balances the electric force [15], [16]. The crystal formation also requires an inward radial force to balance the mutual repulsion of the negatively charged particles. In previous experiments, the powered electrode of the CCP was slightly dished such that the gravitational force provided the critical inward compression of the 5-8 μm particles [17]. Alternately, a retaining ring was place on the

electrode to modify the plasma potential and radially confine particles [18]. In this microplasma, however, we observe crystal formation over a planar, unpowered dielectric. The required inward force on the particles is due to the rapid spatial decay of the microplasma and the resulting radial potential gradient.

C. Particle motion with sheath expansion

The ion drag force moves particles to the edge of the plasma sheath, but negatively charged particles are not able to overcome the strong potential gradient in sheath. In this manner, particles are confined close to the sheath edge. If the sheath is expanded, the particles can be moved. In order to observe this particle motion, we applied a DC signal to the bias T as shown in Fig. 1 to expand sheath. The total signal applied to the SRR consisted of the 900 MHz microwave to sustain the microplasma plus a DC voltage to manipulate the sheath width. A group of photos in Fig. 6 shows particle motion in 2 Torr argon microplasma with an applied voltage that is ramped from -60 V to 60 V. Photo (a) in Fig. 6 was taken at -60 V. Since the SRR electrodes were negatively biased, the sheath adjacent to the ring was expanded and particles were pushed toward the grounded reference electrode. When the bias voltage was changed to -20 V as shown in (b), the sheath width near the powered SRR electrode decreased, and particles were pushed back toward the SRR electrode. Since the SRR electrode was still negatively biased, the particles' movement was small. In (c), the bias voltage was 20 V, and the grounded electrodes were negatively biased relative to positively biased SRR electrode. The sheath around the grounded electrodes was expanded and the particles were pushed toward the SRR electrode by the potential gradient in sheath. At the left corner of (c) is an enlarged figure showing particle motion induced by the expanding sheath. Finally the bias voltage reached 60 V as shown in (d). This case was similar to (a), except the particles were trapped close to the SRR electrode. It is important to note that since the particles are held near the sheath edge, the particles' spatial distribution indicates the sheath width. In order to deduce the ion density, the sheath width was measured as a function of bias voltage from Fig. 6. For example, when the bias voltage is 60 V, the sheath width S is 300 μm. The corresponding ion density can be estimated using the collisional sheath [20]:

$$en_s u_s = (\frac{2}{3})(\frac{5}{3})^{3/2}\epsilon_0(\frac{2e\lambda_i}{\pi M})^{1/2}\frac{V_0^{3/2}}{S^{5/2}} \tag{2}$$

where

$$u_s = \frac{u_B}{(1+\pi\lambda_{Ds}/2\lambda_i)^{1/2}}$$

$$u_B = \sqrt{\frac{eT_e}{M}}$$

$$\lambda_{Ds} = (\frac{\epsilon_0 T_e}{en_s})^{1/2}$$

$$\lambda_i = \frac{1}{n_g\sigma_i} \approx \frac{1}{330p}cm$$

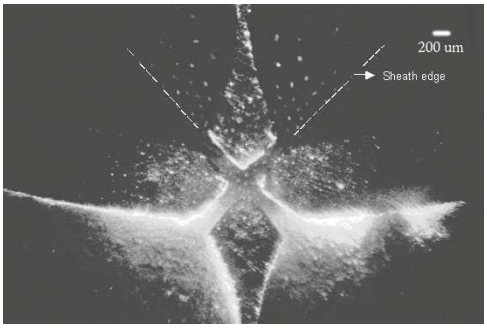

(a) Biased voltage = -60 V

(b) Biased voltage = -20 V

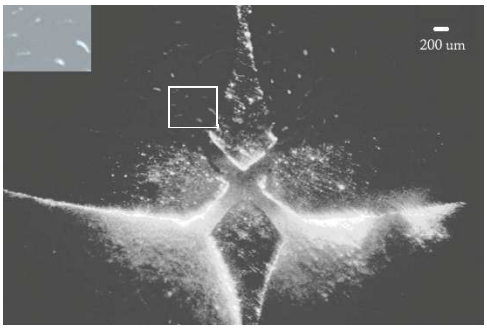

(c) Biased voltage = 20 V

(d) Biased voltage = 60 V

Fig. 6. Particles motion under different bias voltage: (a) Bias voltage =-60 V (b) Bias voltage =-20 V (c) Bias voltage = 20 V (d) Bias voltage = 60 V

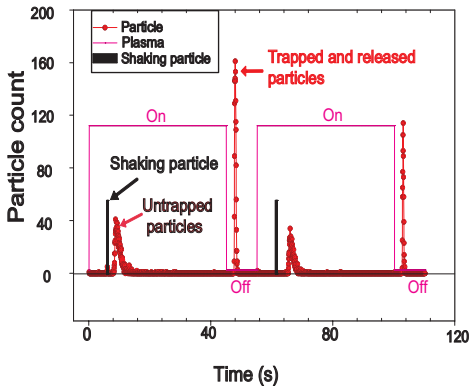

Fig. 7. Example of two experimental cycles

M is the mass of argon, p is 2 Torr, V_0 is ~ 60 V. The result showed $n_i = 1.1 \times 10^{11} cm^{-3}$, which is close to the Langmuir probe measurement (see Table 1).

D. Particle detection

In this section we investigate the motion of trapped particles after the microplasma has been extinguished. Transient Langmuir probe measurements show that the microplasma and its intrinsic potential well decay with a time constant on the order of 60 μs. Once the potential well decays, particles are accelerated by the molecular drag force imposed by gas flowing from inlet 2 toward the vacuum pump. As an example, two experimental cycles are shown in Fig. 7. The plasma was turned on by a RF relay, which was controlled by Labview, and microparticles were shaken into the microplasma after 6 s. A few seconds later, untrapped particles were detected by an in-line laser particle counter as shown in Fig. 1. After 45 s, the plasma was turned off, such that trapped particles were released from plasma and detected by particle counter. Fig. 8 shows the normalized particle distributions versus gas flow velocity. The gas velocity was modified by varying the pressure from 1.6 to 1.9 Torr at a fixed argon flow of 1.65 sccm. Table 2 shows the time-of-flight as a function of gas velocity through the plasma. The product of gas velocity (v) and time-of-flight (t_f) consistently indicates the separation between the microplasma trap and the particle sensor port. After the microplasma is extinguished, the particle motion is dominated by the molecular drag force.

TABLE II
TIME-OF-FLIGHT AND FLIGHT DISTANCE VERSUS GAS FLOW VELOCITY

Gas velocity, $v(cm/s)$	Time-of-flight, t_f(s)	$t_f v(cm))$
1.17	2.9	3.39
1.11	3.1	3.44
1.05	3.25	3.41

E. Time-of-flight under static electric field

If the microplasma is to replace radio isotopes in particle detectors, it is necessary that the particles retain their plasma-induced negative charge during and after plasma decay. In this

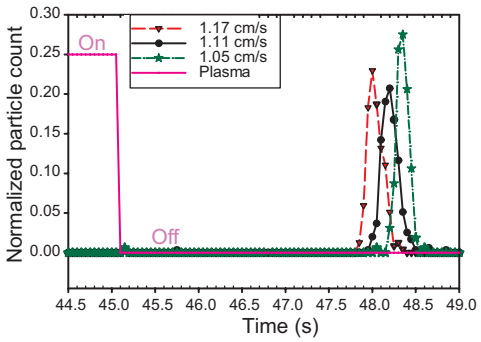

Fig. 8. Particle distribution versus gas flow velocity

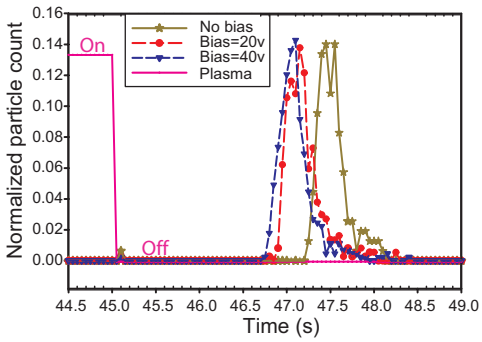

Fig. 9. Particle distribution versus bias voltage

section, we attempt to modify the time-of-flight by applying a positive voltage to the SRR shortly after the power has been turned off and the microplasma has decayed. Here we still seeded the microplasma with particles, waited 45 s, and then turn the plasma off. Next, after a 0.1 s delay to ensure the plasma has decayed, we applied positive voltage to the SRR to create an electrostatic field that expels negatively charged particles. Experimentally, we observed a shorter time-of-flight for particles that were accelerated by this electrostatic field (See Fig. 9). This demonstrates that particles remain negatively charged after the plasma decays and that the particles can potentially be manipulated, sorted and detected by their charge.

IV. CONCLUSION

Charging and trapping of gas-borne particles using a microplasma was introduced. Microparticles were suspended above an unbiased dielectric substrate by the strong potential gradient between the substrate and the microplasma. Simultaneously, the weaker potential gradient at the microplasma's unbounded edge was sufficient to trap the microparticles against the molecular drag force of flowing argon.

A bias voltage was applied to the entire SRR structure to expand the plasma sheath, and microparticle motion with sheath expansion was observed. The sheath width was determined by the positions of the trapped particles, and the ion density deduced from the sheath width is the order of 10^{11} cm^{-3}.

After plasma extinction, the trapped particles were released and carried by molecule drag force to the gas outlet where

they were detected by a laser particle counter. The particles' time-of-flight is inversely proportional to gas flow velocity indicating that molecular drag forces dominate particle motion in the absence of the microplasma. The charge on the particles persists after the microplasma has been turned off, allowing the particles to be manipulated by external electric fields, such as those encountered in differential mobility analyzers.

ACKNOWLEDGEMENT

This work was supported by the National Science Foundation Grant No. CCF-0403460.

REFERENCES

[1] B. Y. H. Liu and D. Y. H. Pui, "Equilibrium Bipolar Charge Distribution of Aerosols," J. of Coll. Interface Sci., vol. 49, pp. 305-312, 1974.

[2] A. Wiedensohler, E. Lütkemeier, M. Feldpausch, and C. Helsper, "Investigation of the Bipolar Charge Distribution at Various Gas Conditions," Journal of Aerosol Science, vol. 17, pp. 413-416, 1986.

[3] G. Praburam and J. Goree, "Observations of particle layers levitated in an rf sputtering plasma," J. Vac. Sci. Technol. A, vol. 12, pp. 3137-3145, 1994.

[4] G. S. Selwyn, J. Singh, and R. S. Bennett, "In Situ laser diagnostic studies of plasma-generated particulate contamination," J. Vac. Sci. Technol. A, vol. 7, p. 2758, 1989.

[5] E. Whipple, "Potentials of surfaces in space," Rep. Prog. Phys., vol. 44, pp. 1197-1250, 1981.

[6] J. Goree, "Charging of particles in a plasma," Plasma Sources Sci. Technol., vol. 3, no. 3, pp.400-406, Aug. 1994.

[7] S. J. Choi and M. J. Kushner, "A particle-in-cell simulation of dust charging and shielding in low pressure glow discharges," IEEE Trans. Plasma Sci., vol. 22, p. 138, 1994.

[8] M. S. Barnes, J. H. Keller, J. C. Forster, J. A. O'Neill, and D. K. Coultas, "Transport of dust particles in glow-discharge plasmas," Phys. Rev. Lett., vol. 68, p. 313, 1992.

[9] K. Ostrikov and L. Stenflo, "On equilibrium states and dust charging in dusty plasmas," IEEE Trans. Plasma Sci., vol. 29, p. 175, 2001. Also, see P. K. Shukla, D. Mendis, and V. W. Chow, The Frontiers of Dusty Plasmas. Singapore: World Scientific, 1996.

[10] V. Karanassios, "Microplasmas for chemical analysis: analytical tools or research toys?" Spectrochem. Acta B, vol. 59, pp. 909-928, 2004.

[11] R. Mohan Sankaran, D. Holunga, R. C. Flagan, K. P. Giapis, "Synthesis of blue luminescent Si nanoparticles using atmospheric-pressure microdischarges," Nano Lett., vol. 5, pp. 537-541, 2005.

[12] J. Hopwood, F. Iza, S. Coy, and D. Fenner, "A microfabricated atmospheric-pressure microplasma source operating in air," J. Phys. D: Applied Physics, vol. 38, pp. 1698-1703, 2005.

[13] C. Cui and J. Goree, "Fluctuations of the Charge on a Dust Grain in a Plasma," IEEE Trans. Plasma Sci., vol. 22, no. 2, pp. 151-158, 1994.

[14] M. A. Lieberman and A. J. Lichtenberg, Principles of Plasma Discharges and Materials Processing 2nd Ed., p. 167, Wiley, 2005.

[15] J. F. O'Hanlon, J. Kang, L. K. Russell, and L. Hong, "The effects of electrostatic, molecular drag, and gravitational forces on the behavior of particle clouds in an RF discharge," IEEE Trans. Plasma Sci., vol. 22, no. 2, pp. 122-127, 1994.

[16] S. J. Choi and M. J. Kushner, "A particle-in-cell simulation of dust charging and shielding in low pressure glow discharges," IEEE Trans. Plasma Sci., vol. 22, no. 2, pp. 138-150, 1994.

[17] G. A. Hebner, M. E. Riley, D. S. Johnson, Pauline Ho, and R. J. Buss, "Direct Determination of Particle-Particle Interactions in a 2D Plasma Dust Crystal," Phys. Rev. Lett., vol. 87, pp. 235001-1 2001.

[18] Vivek Vyasa, Gregory A. Hebner, and Mark J. Kushner, "Self-consistent three-dimensional model of dust particle transport and formation of Coulomb crystals in plasma processing reactors," J. Appl. Phys., vol. 92, pp. 6451-6460, 2002.

[19] Felipe Iza, "Design, Fabrication and Modeling of Microfabricated Inductively Coupled Plasma Sources" Master's thesis, Northeastern University, 2000.

[20] M. A. Lieberman and A. J. Lichtenberg, Principles of Plasma Discharges and Materials Processing 2nd Ed., pp. 184, Wiley, 2005.